Methods of Single-Channel Digital Holography for Three-Dimensional Imaging

Roy Kelner and Joseph Rosen

***Abstract*—Digital holography is an effective tool for imaging three-dimensional (3-D) scenes or objects. In this paper, recently developed methods of single channel digital holography are reviewed: the joint object reference digital interferometer (JORDI), Fresnel incoherent correlation holography (FINCH), and Fourier incoherent single channel holography (FISCH).**

***Index Terms*—Holography, optical microscopy, spatial light modulators (SLMs).**

I. Introduction

HOLOGRAPHY is well recognized by its ability to image three-dimensional (3-D) objects, which can later be reconstructed from the recorded hologram [1]. In digital holography, the traditional photographic plate is commonly replaced by a pixelated image sensor [e.g., a charge-couple device (CCD)] and the reconstruction process is performed numerically, using a computer [2]. A well-known digital holography technique that requires only a single photodetector is optical scanning holography [3], which can be used to record information coherently or incoherently. Various methods of spatially incoherent digital holography have been presented, capable of recording holograms of different types, such as Fresnel (e.g., [4], [5]) and Fourier (e.g., [6]–[9]). Some of these are suitable for fluorescence microscopy (e.g., [10], [11]) and may be used to map microscopic [12] or to track macroscopic [13] objects. Interestingly, methods of spatially incoherent holography may have improved lateral resolution [11], [14].

This paper is a followup to an invited review paper [15] for the 13th IEEE International Conference on Industrial Informatics (INDIN 2015). It is an extended version, with completely revised text and many new experimental results. It summarizes some of the research in which we have been involved in recent years. The next section describes the joint object reference digital interferometer (JORDI), and is followed by sections dedicated to the Fresnel incoherent correlation holography (FINCH), an optical sectioning capable configuration of FINCH, and finally the Fourier incoherent single channel holography (FISCH). These three methods of holography are realized in the form of a single-channel interferometer (i.e., a common-path optical interferometer in which the interfering beams of light always travel together, with a common direction) and use spatial light modulators (SLMs). While FINCH and FISCH are methods of spatially incoherent holography, JORDI is a coherent method.

Manuscript received June 29, 2015; revised August 19, 2015; accepted August 19, 2015. Date of publication September 01, 2015; date of current version February 02, 2016. This work was supported in part by the Israel Ministry of Science and Technology (MOST) and in part by the Israel Science Foundation (ISF) (439/12). Paper no. TII-15-1037.

The authors are with the Department of Electrical and Computer Engineering, Ben-Gurion University of the Negev, Beer-Sheva 8410501, Israel (e-mail: kelnerr@post.bgu.ac.il; rosen@ee.bgu.ac.il).

Color versions of one or more of the figures in this paper are available online at http://ieeexplore.ieee.org.

Digital Object Identifier 10.1109/TII.2015.2475247

II. Joint Object Reference Digital Interferometer

The development of JODRI [16]–[18], which is a system capable of recording holograms of various types under coherent illumination, was partly inspired by Gabor's holographic method [1]. On one hand, both systems have a single channel (in-line) setup, which offers some nice qualitative characteristics. On the other hand, JORDI offers the possibility to overcome what may be considered two main limitations of the Gabor implementation, namely the weak-scattering condition and the twin-image problem. The latter raises at the hologram recording stage, where the recorded intensity of the interference pattern (i.e., the hologram) is

$$I = |u_{\text{obj}} + u_{\text{ref}}|^2 = |u_{\text{obj}}|^2 + |u_{\text{ref}}|^2 + u_{\text{obj}} u_{\text{ref}}^* + u_{\text{obj}}^* u_{\text{ref}} \quad (1)$$

where u_{obj} and u_{ref} represent the object scattered and reference waves, respectively, upon reaching the hologram plane. The third term in the right-hand side of (1) is a desired term that contains the complex information of the object, multiplied by a known reference. The other terms in the right-hand side constitute the zeroth order term (two leftmost terms) and a term conjugated to the desired term (rightmost term), which represents the twin image. Commonly, information from these two terms overlaps with the information of the desired term, hence limiting the quality and visibility of the desired term holographic reconstruction. The weak-scattering condition assumes that two mutually coherent waves are emitted from the illuminated object, one that does not contain any spatial information and is relatively intense, which can serve as the reference u_{ref}, and another that contains the spatial information of the object u_{obj}, and is of a relatively low intensity. Thus, any object that does not satisfy this condition cannot be successfully recorded.

In JORDI, the weak-scattering condition is relieved. Instead, it is assumed that the wave entering the system can serve both as the object and reference waves. The latter only requires a part of the wavefront at the system input plane to carry no information that is related to the object, as is explained shortly. A schematic of the first JORDI design is presented in Fig. 1, where a collimated laser beam is used to illuminate an object. The actual

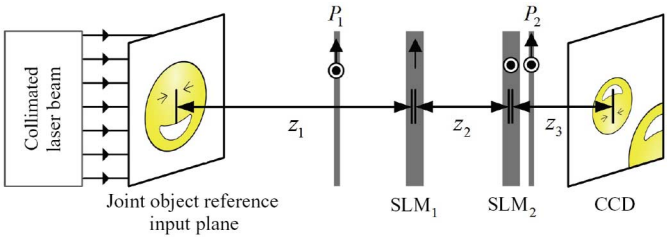

Fig. 1. Schematic of the first JORDI recorder [16]. P_1 and P_2, polarizers; SLM$_1$ and SLM$_2$, spatial light modulators; CCD, charge-coupled device.

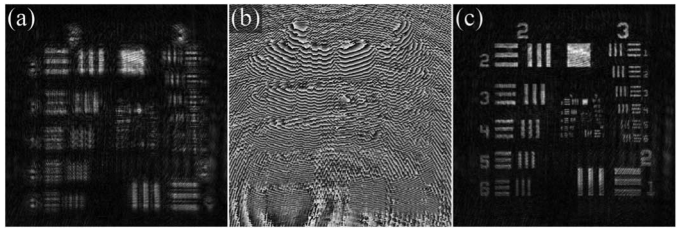

Fig. 2. Experimental results from a JORDI recorder based on Fig. 1. (a) Amplitude and (b) phase of the recorded hologram, following a phase-shifting procedure. (c) Hologram reconstruction at plane of best focus.

system is realized using two phase-only SLMs, positioned with their active axes perpendicular to each other. A polarizer is placed before the SLMs; usually, with its transmission axis oriented at a 45° angle to the active axes of the SLMs. The SLMs used are sensitive to polarization, in the sense that polarization components of light that are oriented along the SLM active axis experience varying refractive indices, which are electronically controlled for each pixel of the SLM, while polarization components of orthogonal orientation, along the SLM nonactive axis, experience a uniform refractive index. That is, each pixel of the SLM can be set to induce a relative phase retardation of a controllable degree, ideally, between zero and 2π (up to a full wavelength). Alternatively, it is possible to say that when a beam of light passes through the SLM, its polarization components that are oriented along the SLM active axis are modulated, while the orthogonal components are not.

According to the above principle, the two SLMs in Fig. 1 can be used to control two orthogonal polarization components of light. Therefore, if a lens is displayed on each of the SLMs, two separate imaging systems are formed. The two systems coexist in the same physical space, and thus a single channel setup is formed. In JORDI, one of these systems is responsible for imaging the reference part of the input plane onto the detector [e.g., a CCD] plane, and the other is set so that one of various types of holograms is formed. The role of the second polarizer P_2 is to project the two orthogonal polarization components of the two imaging system into a common orientation, enabling interference between the two.

Here, a specific configuration of JORDI that can be used to form an image hologram of a transmissive object is discussed. The idea is to simultaneously form overlapping images of the object and the reference on the CCD plane, as depicted in Fig. 1, in which an image of the object is formed using SLM$_2$ and a laterally displaced image of the reference is formed using SLM$_1$. It is required that as the collimated laser beam illuminates the object, it is also allowed to freely pass at a certain region of the input plane. This region can readily serve as the source for the reference wave. SLM$_1$ is located at distances of z_1 and $z_2 + z_3$ from the input and CCD planes, respectively. Thus, by displaying a mask of a lens on this SLM an image of the input plane can easily be formed on the CCD, granted that the focal length of this lens f_1 is

$$f_1 = z_1 (z_2 + z_3)/(z_1 + z_2 + z_3). \tag{2}$$

Note that the lateral magnification of this system is equal to $m_1 = -(z_2 + z_3)/z_1$. As for SLM$_2$, which is located at distances of $z_1 + z_2$ and z_3 from the input and CCD planes, respectively, the focal length f_2 of the lens that is displayed should be

$$f_2 = (z_1 + z_2)\, z_3/(z_1 + z_2 + z_3) \tag{3}$$

giving rise to a lateral magnification of $m_2 = -z_3/(z_1 + z_2)$.

In order to achieve the desired overlap between the images of the reference and the object, the size of the reference image must be equal to or larger than the size of the object image. This can be achieved through proper positioning of the two SLMs, through which the relative lateral magnification between the two imaging system m_2/m_1 can be controlled. This is an important degree of freedom that indicates that the size of the object and the reference in the input plane need not be similar. Additionally, lateral displacement of either of the images may be necessary in order for them to overlap. This can be achieved electronically, through a lateral displacement of the SLM displayed lens. However, in practice, it may be best to keep the object and its image centered, to avoid loss of resolution due to an asymmetrical imaging lens. The reference, on the other hand, does not carry spatial information from the object. Two important aspects in this configuration include the twin-image problem and the relative intensity between the reference and object. If necessary, the latter can be controlled by changing the orientations of the polarizers P_1 and P_2 (Fig. 1). As for the twin-image problem, either of the SLMs can also be used as a phase-shifting device, adding a constant phase term to its modulated wave and enabling the execution of a phase-shifting procedure [2] for the removal of the zeroth order term and the twin. For example, by adding a constant phase term to the reference, (1) can be written as

$$I_k = |u_{\text{obj}}|^2 + |u_{\text{ref}}|^2 + e^{-i\theta_k} u_{\text{obj}} u^*_{\text{ref}} + e^{i\theta_k} u^*_{\text{obj}} u_{\text{ref}} \tag{4}$$

where $\theta_k = 2\pi k/3$, with $k = 0, 1, 2$, meaning that three holograms are recorded with different constant phase terms. Then, a complex-valued hologram that only contains the desired term is formed by a proper linear combination of the three holograms. It is important to emphasize that JORDI can also be used to record off-axis holograms (as an alternative to a phase-shifting procedure), and Fresnel or Fourier holograms. Some of these were demonstrated in [16].

Experimental results from a JORDI system based on Fig. 1 are presented in Fig. 2. The system was implemented using a Melles Griot HeNe laser (central wavelength $\lambda = 632.8$ nm), two Holoeye PLUTO SLMs (1920 × 1080 pixels, 8 μm pixel

pitch, phase-only modulation) and a PCO Edge scientific complementary metal-oxide semiconductor (sCMOS) camera (2560×2160 pixels, $6.5\,\mu$m pixel pitch, monochrome). Note that the phase-only SLMs used here, and throughout this paper, are not transmissive, as shown in the figures for simplicity, but are actually reflective. In [16], the SLMs were approached at a small incident angle. Here, a beam-splitter was located in front of each SLM, positioning the SLM orthogonally to the optical axis, as shown in [17, Fig. 2]. This setup tradesoff light efficiency for ideal positioning of the SLMs. In light demanding applications, the former may be preferred, unless transmissive phase-only SLMs become available. The parameters in the system were $z_1 = z_2 = 20\,$cm and $z_3 = 40\,$cm. f_1 and f_2 were determined according to (2) and (3), respectively; for the latter, and for the sake of demonstration, a z_3 value of 42 cm was used instead of 40 cm. A negative 1951 United States Air Force (USAF) resolution chart (Thorlabs R3L3S1N) served as a target. The reference region was constrained to the clear rectangular area between element 2 of group 0 and element 1 of group 1 of the USAF chart. Following a phase-shifting procedure, a complex hologram was formed using three raw holograms. Its amplitude and phase are shown in Fig. 2(a) and (b), respectively. Although the object is out of focus, it can be focused by Fresnel back propagation. The hologram reconstruction is shown in Fig. 2(c), implying upon the reliability of the acquired amplitude and phase information.

The resolution of the first JORDI recorder [16], which constitutes a refractive lens-free design, is rather limited by the achievable numerical aperture (NA) of the SLM realized diffractive lens, which is much lower than the NA that may be offered by a refractive lens (e.g., by a microscope objective). A converging (i.e., positive) lens of a focal length f can be modeled by the quadratic phase function

$$Q\left(-1/f\right) = \exp\left[-\left(x^2 + y^2\right) i\pi/(\lambda f)\right] \tag{5}$$

where λ is defined as the central wavelength of the coherent laser illumination and (x, y) are Cartesian coordinates of the lens plane, with the lens centered to the origin coordinate (0,0). To display this lens on a phase-only SLM, the 2π modulus of the argument is usually calculated, sampled according to the coordinates of the SLM pixels. However, it is clear that the frequency of the modulus of this quadratic function rises quite rapidly with respect to the distance from the origin (0,0). The lens can be faithfully displayed on the SLM only if it is properly sampled, according to the well-known Nyquist criterion, which states that the function sampling frequency should be twice as high as the highest frequency of the function. In practice, current commercially available phase-only SLMs can be used to display lenses with a NA value of roughly up to 0.035, easily an order of a magnitude less than readily available refractive lenses.

A more recent design of JORDI [17] overcomes the above limitation by incorporating a refractive objective lens into the system. A schematic of the configuration is depicted in Fig. 3. Based on reasoning similar to that has been used to explain the previous JORDI design (Fig. 1), here, a two lens system is formed by the objective lens L_o together with each of the SLMs. As before, the two systems share the same physical

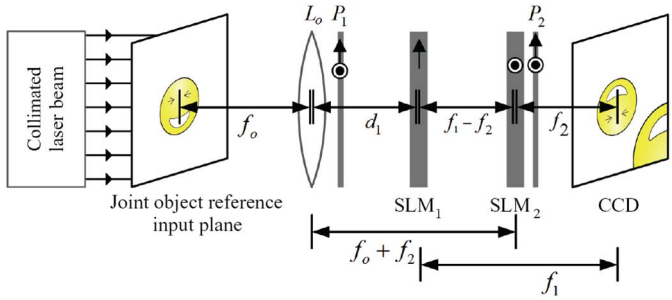

Fig. 3. Schematic of a JORDI recorder [17]. L_o, objective lens; P_1 and P_2, polarizers; SLM$_1$ and SLM$_2$, spatial light modulators; CCD, charge-coupled device.

path, together forming a single-channel common-path interferometer. Fig. 3 demonstrates the recording process of an image hologram, where the object is imaged to the CCD plane via the afocal system that is formed by the objective lens and by SLM$_2$. The lateral magnification of this system is $m_2 = -f_2/f_o$, where f_o and f_2 are the focal lengths of the objective lens L_o and the lens displayed on SLM$_2$, respectively. Simultaneously, an image of the reference is formed by the two lens imaging system comprised of the objective lens and SLM$_1$. This system is not afocal, yet maintains a lateral magnification of $m_1 = -f_1/f_o$, where f_1 is the focal length of the lens displayed on SLM$_1$. The latter is not necessarily centered around the optical axis, so that the reference can be properly overlaid on the image of the object. In this setup, the relative lateral magnification between the two imaging system is $m_2/m_1 = f_2/f_1$. Once again, the size of the object and the reference regions within the input plane need not be equal. If necessary, a phase-shifting procedure can be applied to eliminate the zeroth order and twin-image terms.

In [17], the proposed JORDI configuration was analytically and experimentally shown to satisfy the Abbe resolution criterion of a coherent imaging system [19], according to which the minimum resolvable distance between a pair of grating lines at the input plane of the system is

$$\Delta_{\min} = 0.82\lambda/\mathrm{NA} \tag{6}$$

where $\mathrm{NA} = D/(2f_o)$ is the numerical aperture of the system. The parameter D is the size of the system aperture. Furthermore, the system was tested with transmissive and reflective objects of various types (e.g., binary, highly scattering, and phase-mostly objects), and was also shown to work using a microscope objective. In Fig. 4 [15], results taken with a JORDI recorder that uses a microscope objective (Newport M-10X, NA of 0.25, $f_o = 16.5\,$mm) are shown. A negative 1951 USAF resolution chart (Thorlabs R3L3S1N) was placed at a small distance next to the input plane (Fig. 3), in order to enable the demonstration of digital focusing into a desired plane. Ideally, a two-dimensional (2-D) object should be positioned exactly in the input plane for best resolution. In the final complex hologram [Fig. 4(a) and (b)] (following a phase-shifting procedure), the resolution chart is out of focus. Still, since the hologram contains both amplitude and phase information, a digital Fresnel back propagation hologram

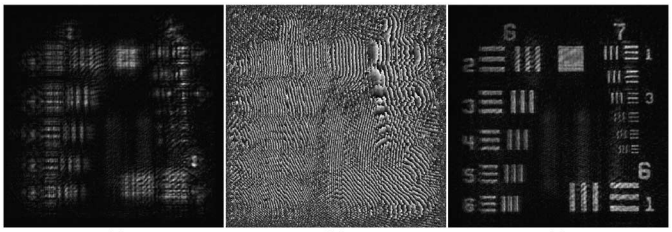

Fig. 4. Holographic microscopy using JORDI [15]. (a) Amplitude and (b) phase of the recorded hologram, following a phase-shifting procedure. (c) Hologram reconstruction of a negative 1951 USAF resolution chart, revealing details of resolution groups 6 and 7 at up to 228 line pairs per millimeter.

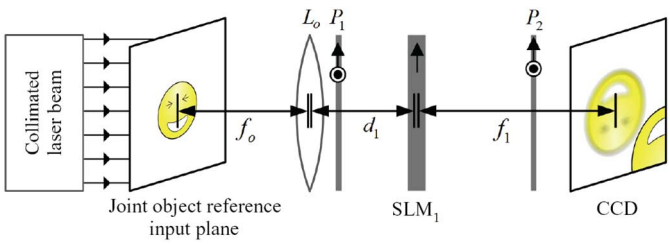

Fig. 5. Schematic of a JORDI recorder based on a single SLM [18]. L_o, objective lens; P_1 and P_2, polarizers; SLM$_1$, spatial light modulator; CCD, charge-coupled device.

reconstruction is easily performed to reveal the in-focus details of the chart [Fig. 4(c)].

As previously stated, the JORDI designs of [16] and [17] can be set to achieve a desired relative lateral magnification between the object and reference channels. In general, this is an important degree of freedom, but it can be waived if the reference region in the joint object reference input plane is large enough, relative to the object region. This offers the opportunity to implement JORDI using only a single SLM, as done in [18] and shown in Fig. 5, where the imaging system formed by the objective lens and the SLM is used to image the reference onto the CCD plane. As for the object, it is no longer imaged onto the CCD plane, but its information (in Fresnel or Fourier space, depending on the distance between the objective lens and the CCD) is encoded into the hologram, as long as the reference region is large enough. Geometrical considerations can show that the reference and object region at the input plane should be of comparable sizes. It is important to note that all of the above designs of JORDI image the reference onto the CCD plane. This assures that the separation between the object and reference that exists in the input plane is preserved in the CCD plane, even though the shape of the reference itself may be changed from a plane wave into a spherical wave (which can be compensated for, if needed, after the hologram is acquired).

Experimental results acquired with a setup based on Fig. 5 are presented in Fig. 6. The system was implemented using a microscope objective (Nikon Plan Apo 20x DIC M, NA of 0.75). Other parameters were $d_1 = 15\,\text{cm}$ and $f_1 = 40\,\text{cm}$. A positive high-frequency National Bureau of Standards (NBS) 1963A resolution chart (Thorlabs R2L2S1P1) was positioned at the front focal plane of the objective lens. A complex hologram was acquired using a phase-shifting procedure; its amplitude

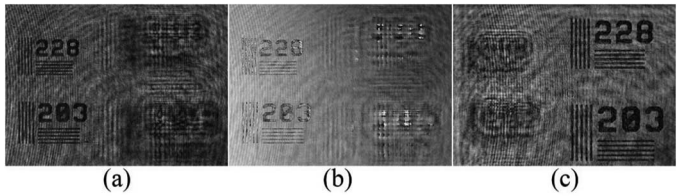

Fig. 6. Single SLM JORDI experimental results. (a) Amplitude and (b) phase of the hologram, following phase-shifting. (c) Hologram reconstruction of the resolution chart, at plane of best focus of the right-hand-side part.

and phase (digitally compensated for spherical curvature) are shown in Fig. 6(a) and (b), respectively. The right-hand-sides of these figures represent a Fresnel hologram. Its reconstruction at plane of the best focus is shown in Fig. 6(c). Note that the left-hand-sides of these figures represent an image hologram.

III. Fresnel Incoherent Correlation Holography

FINCH was introduced in 2007 by Rosen and Brooker [4] as a common-path single-channel interferometer capable of recording Fresnel holograms under spatially incoherent illumination conditions. Soon after, a FINCH configuration capable of recording colored holograms of fluorescent objects was proposed and demonstrated [20]. Naturally, this was promptly extended into a new type of a holographic fluorescence microscope, known as a FINCHSCOPE [10]. Recently, a more light-efficient version of the FINCHSCOPE has been introduced [21]. The added light efficiency in the updated design is achieved by using a transmissive liquid crystal gradient index lens, rather than a reflective SLM, as commonly used in FINCH. FINCH, FINCH-related, and other systems of spatially incoherent digital holography have been widely explored in the last years (e.g., [5], [14], [22]–[47]). The contributions of these works cover various grounds, including theoretical aspects and system modifications. The self-interference incoherent digital holography (SIDH) [5], [35], [40] and FINCH are based on similar working concepts. Unlike FINCH, SIDH possesses the dual-channel structure of modified Michelson interferometer, in which the two plane mirrors are replaced with spherical mirrors of different curvatures. SIDH was successfully utilized for adaptive optics [5] and natural light holography [35]. In [34], the field of view (FOV) in FINCH-based microscopy is investigated and a modification to the design, capable of providing an extended FOV, is suggested. Telescopic configurations of FINCH—specifically intended for observing far away objects—capable of synthetic aperture imaging, with improved system resolution, were suggested in [24] and [45].

Several corner-stone configurations of FINCH are presented in Fig. 7. A simplified schematic of the first FINCH design [4] is shown in Fig. 7(a) and includes: a 3-D object from which spatially incoherent light is either emitted (e.g., a fluorescent object) or scattered; an objective lens L_o, which collects light into the system; a phase-only SLM that serves as a diffractive lens, a beam-splitter, and a phase-shifting procedure enabling device; an input polarizer P_1 oriented with accordance to the active axis of the SLM, so that most (ideally, all) of the light is

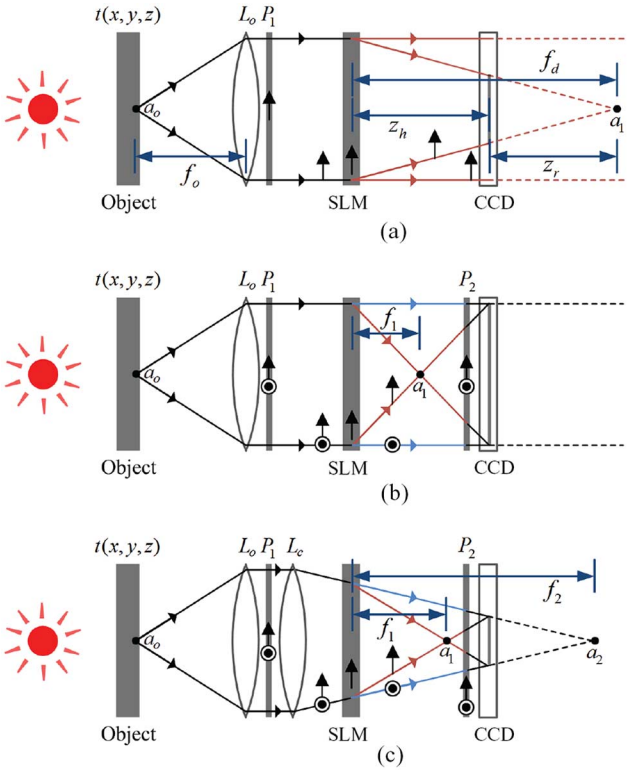

Fig. 7. Simplified schematics of various FINCH configurations. (a) In the first configuration of FINCH [4], the spatial multiplexing method is used to display two diffractive optical elements over the SLM, a lens and a clear aperture. The object is simultaneously imaged to infinity and to a location behind the CCD. Each pair of interfering beam, originating from a single point source, does not perfectly overlap on the CCD plane. (b) More recent design [14] uses the polarization method [23] which enables utilizing all SLM pixels for displaying a lens. The object is simultaneously imaged to infinity and to a central location between the SLM and the CCD, satisfying the perfect overlap condition and achieving optimal resolution. (c) Diffractive/refractive dual-lens FINCH configuration (first demonstrated in [50]) uses the polarization method. The object is simultaneously imaged into two locations, before and after the CCD, reducing OPD while satisfying the perfect overlap condition and maintaining optimal resolution. L_o, objective lens; P_1 and P_2, polarizers; SLM, spatial light modulator; CCD, charge-coupled device. A BPF, not shown in the schematics, may be incorporated to assure sufficient temporal coherence, depending on the specific illumination conditions.

modulated by the SLM; a detector (e.g., CCD or CMOS), which is used for recording the hologram. The common-path single-channel structure of FINCH is apparent. In this interferometer, it is assumed that the object consists of spatially incoherent point sources, and thus light that originates from a specific point source cannot interfere with light from other points; nor can it interfere with a reference wave of a different origin. In FINCH, instead, each point source is made to interfere with itself. The intensity of this interference pattern is recorded by the CCD in the form of a hologram. Following a phase-shifting procedure [4], a complex hologram is calculated. For a single point source, the hologram holds the form of a diffractive lens. The intensity and 3-D position of the point are encoded into the parameters of this lens (i.e., focal length, central position, and transmittance). For many point sources, under the spatial incoherence assumption, the recorded hologram is actually a summation over the intensity contributions of all point sources. It should be noted that the self-interference-based approach to incoherent holography was suggested and demonstrated half a century ago in [48] and [49], respectively.

More specifically, consider the case of a spherical wave emitted from a point source object located at the front focal plane of the objective lens L_o, in the lateral location $\vec{r}_s = (x_s, y_s)$, as depicted in Fig. 7(a). This wave is transformed into two mutually coherent waves: a spherical wave and a tilted plane wave. The former can be represented on the CCD plane as

$$u_1(x,y;\vec{r}_s) = e^{i\theta_k} c_1(\vec{r}_s)\sqrt{I_s(\vec{r}_s)}L[-f_d\vec{r}_s/(f_o z_r)]\,Q\,(-1/z_r) \tag{7}$$

where f_o and f_d are the focal lengths of the objective lens L_o and the SLM displayed diffractive lens, respectively, z_r is the distance between the CCD and the image point a_1, c_1 is a complex valued constant, dependent on the point source position, $L[\vec{s} = (s_x, s_y)] = \exp[i2\pi\lambda^{-1}(s_x x + s_y y)]$ is a linear phase function, I_s is the point source intensity, and $\exp(i\theta_k)$ is a constant phase term used in the phase-shifting procedure, commonly with $\theta_k = 2\pi k/3,\ k = 0, 1, 2$. The tilted plane wave can be represented on the CCD plane as

$$u_2\,(x,y;\vec{r}_s) = c_2\,(\vec{r}_s)\,\sqrt{I_s\,(\vec{r}_s)}L\,(-\vec{r}_s/f_o) \tag{8}$$

where c_2 is a complex valued constant. The recorded hologram is the intensity of the interference of the waves described in (7) and (8)

$$\begin{aligned} h\,(x,y;\vec{r}_s) &= |u_1\,(x,y;\vec{r}_s) + u_2\,(x,y;\vec{r}_s)|^2 \\ &= I_s\,(\vec{r}_s)\left[|c_1\,(\vec{r}_s)|^2 + |c_2\,(\vec{r}_s)|^2\right] \\ &\quad + I_s\,(\vec{r}_s)\left[e^{i\theta_k} c_1\,(\vec{r}_s)\,c_2^*\,(\vec{r}_s)\,L\left(\frac{z_r - f_d}{f_o z_r}\vec{r}_s\right)\right. \\ &\quad \left. Q\left(-\frac{1}{z_r}\right) + \text{c.c.}\right] \end{aligned} \tag{9}$$

where c.c. represents the complex conjugate of the expression before it. The three terms in the right-hand-side of (9) represent, from left to right, a zeroth-order term, a desired quadratic phase term that encodes the intensity and the spatial location of the point source, and a conjugated term that represents the twin-image. Following a phase-shifting procedure [4], only the desired quadratic phase term is left. This is analogous to the procedure previously described in the context of (4). However, here the two interfering waves cannot be strictly characterized as an object and reference waves. Rather, they both represent the object, meaning that the process is actually self-referencing in nature. Additionally, (9) represents the hologram intensity due to only a single point source, whereas the hologram of (4) represents the complete object. Still, in FINCH, a summation of all intensity patterns due to all point sources is recorded. In the general case, the recorded hologram is

$$H(x,y) = \iiint h(x,y;\vec{r}_s,z_s)dx_s dy_s dz_s \tag{10}$$

where z_s indicates the axial location of a point source, so that the complete 3-D information of the object is encoded into the hologram simultaneously. Digital focusing into different planes

is digitally performed using numerical Fresnel propagation. In the case described in (9), the reconstruction distance is z_r.

It should be noted that to record a hologram with sufficient fringe visibility (meaning that the degree of temporal coherence is high enough), the maximal optical path difference (OPD) between interfering beams $\delta_{\max}$ should satisfy the condition

$$\delta_{\max} \leq \lambda^2/\Delta\lambda \tag{11}$$

where $\Delta\lambda$ is the spectral bandwidth of the source, in terms of wavelengths [51]. The maximal OPD can be determined based on geometrical considerations and can be reduced through a modified realization of FINCH that is described shortly. Whenever necessary, a bandpass filter (BPF) of a narrow enough spectral bandwidth $\Delta\lambda$ may be incorporated into the system. Another important aspect in the system of Fig. 7(a) is the SLM role as a beam splitter. Note the two waves to the right of the SLM in Fig. 7(a). The plane wave that propagates through the SLM is transformed into a spherical wave by the diffractive lens that is displayed on the SLM, but is also allowed to freely pass the SLM. In [4], this was achieved by spatially multiplexing two elements on the SLM, meaning that from all the pixel of the SLM, only a half is used to display the diffractive lens. The pixels are randomly selected and uniformly distributed over the SLM, and the selection is kept throughout the phase-shifting procedure. The other half is used to display a uniform constant phase (preferably, zero). This technique is referred to as "the spatial multiplexing method." The problem with this approach of spatial multiplexing is that each element only occupies half of the SLM aperture and also exhibits many discontinuities. As is shortly demonstrated, this results with many artifacts in the hologram reconstruction.

A solution to the above artifacts problem, as suggested in [23], uses an alternative multiplexing technique referred to as "the polarization method," which is depicted in Fig. 7(b). The method makes use of the birefringence properties of the SLM. Here, the input polarizer P_1 is set so that its transmission axis is oriented at a 45° angle to the active axis of the SLM. Hence, the polarized light that arrives to the SLM can be treated as having components parallel to the active axis of the SLM, and orthogonal components of similar magnitude parallel to the inactive axis of the SLM. Therefore, the SLM realized diffractive lens, which is displayed on the entire SLM, now only affects 50% of the light that propagates through the SLM, resulting with the spherical wave to the right of the SLM [Fig. 7(b)]. The other 50% freely passes through the SLM and are not modulated by it [depicted in Fig. 7(b) as a plane wave to the right of the SLM]. A second polarizer P_2 is inserted in front of the CCD, with its transmission axis also at a 45° degree angle to the SLM active axis, in order to project the two orthogonally polarized waves into a common orientation, and thus allow interference between the two. Note that it is also possible to use angles different from 45° to control the relative intensity of the two waves.

Another important modification suggested in [14], and shown in Fig. 7(b), dictates the focal length of the SLM displayed diffractive lens. This should be set to a value that leads to a perfect overlap between the interfering waves over the CCD plane, which in turn assures optimal resolution. However, the maximal OPD $\delta_{\max}$ in Fig. 7(b) is larger than the one in Fig. 7(a), meaning that the fringe pattern visibility is diminished. This is shown based on geometrical considerations and the approximation $(1+x)^{1/2} \approx 1 + x/2$ (for $x << 1$). The maximal OPD in Fig. 7(a) is

$$\delta_{\max,a} \approx R_{\text{SLM}}^2 z_h / \left(2 f_d^2\right) \tag{12}$$

where z_h is the distance between the SLM and the CCD and R_{SLM} is the SLM aperture radius. The maximal OPD in Fig. 7(b) is

$$\delta_{\max,b} \approx 2R_{\text{SLM}}^2/z_h = R_{\text{SLM}}^2/f_1 \tag{13}$$

where f_1 is the focal length of the SLM realized diffractive lens. Under the condition of perfect overlap between the two waves $f_1 = z_h \ / \ 2$, while in Fig. 7(a) $f_d > z_h$. Rewriting (12) in the form $\delta_{\max,a} \approx R_{\text{SLM}}^2 2f_1/(2f_d^2) = R_{\text{SLM}}^2 f_1/f_d^2$, it is now clear that $\delta_{\max,a}$ is always smaller than $\delta_{\max,b}$, since $f_d > f_1 > 0$.

Different FINCH setups that maintain optimal resolution while offering a reduction in the maximal OPD of (13) were suggested in [14] and [27]. The actual setup depicted in Fig. 7(c) was first demonstrated in [50] and incorporates an additional refractive lens L_c. This setup is configured to form two images of the object in close proximity to the CCD, one before the CCD and one after it (the latter is not actually formed, as the light is blocked by the CCD). This is in contrast to the setups of Fig. 7(a) and (b) where only one of the images is close to the CCD, whereas the other can be considered to be hypothetically formed at infinity. For the simplified case where the distance between the refractive lens L_c and the SLM is zero, the maximal OPD is [27]

$$\delta_{\max,c} \approx R_{\text{SLM}}^2 (f_2 - f_1)/(f_2 f_1) \tag{14}$$

where f_1 and f_2 are the distances between the SLM and the image points a_1 and a_2, respectively. Analysis of (14) indicates that the maximal OPD decreases as f_1 is increased and f_2 is decreased, or in other words, as the distance $f_2 - f_1$ is reduced. In the extreme case of $f_2 \to \infty$, while keeping the perfect overlap condition $z_h = 2f_1 f_2/(f_1 + f_2)$ [27], the setup of Fig. 7(c) degenerates to the setup of Fig. 7(b) (the focal length of the lens L_c is infinity, meaning that L_c can be omitted), and the results of (13) and (14) become equal.

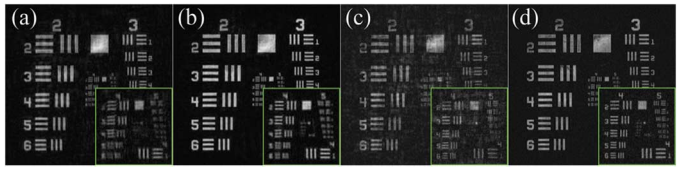

Fig. 8. 1951 USAF resolution chart reconstructions of FINCH holograms at plane of best focus. In (a) and (b), the perfect overlap condition is not satisfied, whereas in (c) and (d) it is. Spatial multiplexing was used for (a) and (c), whereas the polarization method was used for (b) and (d).

Some of the advantages of the above-described modifications of FINCH are experimentally demonstrated in Fig. 8. A FINCH system was built using an objective lens L_o with a focal length of $f_o = 20$ cm, a Holoeye PLUTO SLM and a PCO Edge sCMOS camera. The distance between the SLM and the camera was set to $z_h = 40$ cm. A negative 1951 USAF resolution chart (Thorlabs R3L3S1N) was back illuminated using

a red LED (Thorlabs LED635L, 170 mW, filtered through a BPF of $\lambda = 632.8\,\text{nm}$, $\Delta\lambda = 3\,\text{nm}$). The experimental setup was based either on Fig. 7(a), with $f_d = 60\,\text{cm}$, or on Fig. 7(b), with $f_1 = 20\,\text{cm}$. The latter satisfies the perfect overlap condition. In order to demonstrate the separate contributions of the perfect overlap condition and the polarization method of multiplexing, both of these configurations where tested with the spatial multiplexing method and with the polarization method of multiplexing. The reconstructions of the recorded holograms are presented in Fig. 8(a)–(d). Fig. 8(a) and (b) were recorded with $f_d = 60\,\text{cm}$, so that the achieved resolution is not optimal, whereas Fig. 8(c) and (d) were recorded with $f_1 = 20\,\text{cm}$, satisfying the perfect overlap condition. Indeed, the resolution of the two latter is superior and details of element 3 of group 5 of the 1951 USAF are still resolved. This is in contrast to the two former, where element 5 of group 4 and above are not resolved. As for the two methods of multiplexing, artifacts are prominent in Fig. 8(a) and (c), where the spatial multiplexing method was used. The polarization method is preferred, as Fig. 8(b) and (d) does not exhibit such artifacts. Experimental results with a FINCH system with reduced OPD are presented in [15] and in Section V.

IV. Optical Sectioning Using FINCH

FINCH may be considered appealing to biological applications due to several reasons. First, the 3D information of the object is encoded into the hologram in a manner that allows focusing into different depths after the recording stage has been completed [4], [10], [20], [30]. This ability is common in holography, but since FINCH is intended to work under conditions of spatial incoherence, FINCH is ideal for fluorescent microscopy [10], [20], [21], [23], [30], [38]. Additionally, FINCH has been shown to have superior lateral resolution when compared with classical imaging systems (e.g., a regular microscope) of similar NA [14], [21]. Moreover, thanks to the relatively simple and quite robust single-channel design of FINCH it may be incorporated into existing microscopes. Nevertheless, it is a fairly common situation to experience deterioration in the image quality of an observed plane of focus, due to unfocused light coming from other planes. In certain situations, especially when thick samples are examined, the deterioration in quality may be so severe, rendering the images unsatisfactory. A well-known solution to this problem in microscopy is confocal scanning microscopy [52], a concept developed more than half a century ago. Coherent [53]–[55] and incoherent [56], [57] confocal holographic systems have been since developed.

A confocal configuration of FINCH, suggested in [44], is depicted in Fig. 9. It is based on the FINCH configuration of Fig. 7(c), and incorporates two elements that work in tandem to achieve optical sectioning. Each of these elements is capable of optical sectioning, but the two together enhance this ability. First, instead of illuminating the entire object at once, a point illumination system is configured to illuminate a specific point of interest, namely a_o. Of course, as light penetrates the object other points are also unavoidably illuminated, but ideally to a lesser degree. Notice that the addition of a second

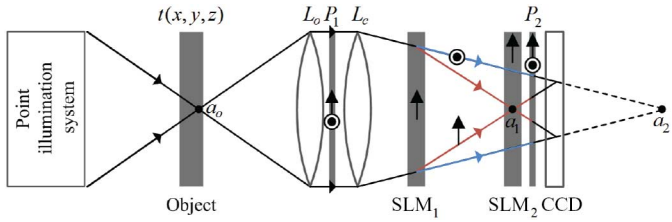

Fig. 9. Schematic representation of a confocal FINCH recorder [44]. L_o, objective lens; L_c, converging lens; P_1 and P_2, polarizers; SLM_1 and SLM_2, spatial light modulators; CCD, charge-coupled device.

phase-only SLM, SLM_2, in an intermediate plane between the first SLM, SLM_1, and the CCD, in which the image point a_1, of the object point of interest a_o, is formed. In conventional (nonholographic) confocal imaging, a pinhole is usually positioned at this point (a_1), allowing light that originates from the object point a_o to freely reach a detector, while blocking light from other regions of the object. Obviously, light from points in the near surroundings of a_o (mostly within the illumination cone of light, shown in Fig. 9) can also pass through the pinhole, but only partially. In FINCH, however, a regular pinhole cannot be simply positioned between SLM_1 and the CCD because it would block the spherical wave that converges into the point a_2 (Fig. 9) from reaching the detector, thus eliminating the holographic process that relies on interference. Instead, it is suggested in [44] to use a "phase pinhole." This element is realized using SLM_2 and imitates an actual pinhole for the waves that form an image of the object in front of the CCD. The polarization direction of these waves is in parallel to the active axes of both SLM_1 and SLM_2. The waves of the orthogonal polarization direction converge toward the image that can hypothetically be formed after the CCD, and are not influenced by the SLMs.

As mentioned, the diffractive optical element displayed on SLM_2 imitates an actual pinhole. It can be described using the following function:

$$G(\vec{r}; r_1) = \begin{cases} \exp(i\theta_k), & |\vec{r}| \le r_1 \\ \exp(i\alpha|\vec{r}|), & \text{otherwise} \end{cases} \tag{15}$$

where $\vec{r} = (x, y)$ and r_1 is the radius of a circular area set to a uniform phase modulation, usually with values of $\theta_k = 0°, 120°,$ and $240°$. The circular area of uniform phase is surrounded by the mask of an axicon $\exp(i\alpha|\vec{r}|)$ where α is a parameter proportional to the axicon angle. The role of the axicon is to deflect light away from the optical system. That is, while an actual pinhole can block light from propagating further and reaching the CCD, the phase pinhole deflects light away from the system, allowing similar effective results. To further enhance the effectiveness of the pinhole, the phase-shifting procedure in the proposed system no longer uses SLM_1. Instead, the small circular area of uniform phase modulation in the phase pinhole mask is used, as described in (15). As the holographic process in FINCH comprises many two waves interactions (i.e., the interference of any two waves that originate from a common point source), any of these which are excluded from the

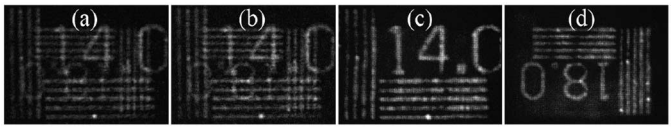

Fig. 10. [15] Optical sectioning using FINCH. (a) and (b) FINCH reconstructions of a 14.0 cycles/mm and 18.0 cycles/mm resolution charts located 30 and 31 cm away from the objective lens, respectively. (c) and (d) Optical-sectioning-FINCH equivalents of (a) and (b), respectively. Note that (a) and (b) result from the same FINCH hologram, whereas (c) and (d) result from two different sets of holograms.

phase shifting (neither of the waves are phase-shifted) would be eliminated from the final complex hologram, mathematically.

The above configuration and procedure can effectively achieve optical sectioning, as is demonstrated shortly. However, most of the information of the object is eliminated from the hologram, and only a specific point of interest is properly encoded into the hologram. Therefore, a scanning process of the plane (or volume) of interest must be applied, just like in confocal scanning microscopy [52]. Thankfully, this can be performed in FINCH without any mechanical movements. The plane of interest in a volume can be chosen by properly adjusting the focal length of the lens displayed on SLM_1, imaging the plane of interest onto the plane of SLM_2. Then, the plane is scanned, point by point, by laterally shifting the phase-pinhole mask. Since many holograms are recorded, each representing a specific point, the reconstruction procedure may become more computationally complex [44]. Note that parallel scanning schemes may be incorporated to ease the process. Recently, another confocal configuration of FINCH, which combines a standard FINCH system with a Nipkow spinning disk has been proposed [46].

Experimental results [44] that demonstrate the optical sectioning capabilities of a phase pinhole-incorporated FINCH (without using a point illumination system) are presented in Fig. 10. [15] Two resolution charts (negative NBS 1963A) were back illuminated using two LEDs (Thorlabs LED635L). A beam-splitter was used to combine the two so that together they form what may be considered a thick object. Its two planes (each resolution chart) were positioned at distances of 30 and 31 cm away from the objective lens. First, a regular (nonsectioning) FINCH hologram was recorded. The hologram reconstructions at the two planes of best focus are presented in Fig. 10(a) and (b). It is quite hard to distinguish between details belonging to either of the resolution charts in these figures. In Fig. 10(c) and (d), however, this is not the case. These figures present reconstructions that result from the scanning process of either planes, using the phase pinhole-incorporated FINCH system. Here, details of the desired plane on interest are clearly visible. It is our belief that the incorporation of optical sectioning capabilities into FINCH is essential for establishing its place in biological microscopy.

V. Fourier Incoherent Single Channel Holography

The FISCH method was introduced three years ago as a method capable of recording digital Fourier holograms under spatially incoherent illumination [6]. Many of its characteristics are prominent in FINCH and include, but are not limited to, the structure of a single-channel incoherent interferometer, achievable lateral resolution that is better by up to a factor of two when compared with a classical imaging system of similar NA, and, of course, the ability to record holograms of spatially incoherent objects. In FINCH, the entire information of the observed 3-D target or scene is encoded into a single real-valued hologram, but a phase-shifting procedure is necessary to overcome the twin-image problem. Thus, at least, three exposures are needed to properly be able to extract the information that is encoded into the hologram, which is of a Fresnel type. In FISCH, a cosine Fourier hologram is recorded, meaning that under certain conditions (such as limiting the observed object into a half plane or space) the entire 3-D information of the recorded object may be extracted from even a single real-valued hologram, rendering the phase-shifting solution unnecessary. Fourier holograms are known to have other beneficial properties. For example, since the information is encoded into Fourier space in the form of cosine fringe patterns, the hologram reconstruction process is somewhat less sensitive to localized information loss, as compared to Fresnel holography.

A simplified schematic of the first FISCH setup is presented in Fig. 11(a). The working principles of FISCH are very close to the ones of FINCH, so the following description is kept brief. Consider a spherical wave that is emitted from the point source a_o of a spatially incoherent object, located at the front focal plane of the objective lens L_o in the coordinate $\vec{r}_s = (x_s, y_s)$. The spherical wave is transformed into a tilted plane wave by the objective and then passes through a linear polarizer oriented at a 45° angle to the active axes of the SLMs (which are set with similar orientation). Converging diffractive lenses are presented on the SLMs, with their focal length f_o set to half of the distance between the SLMs, thereby forming an afocal system that only affects the components of the tilted plane wave along the active axes of the SLMs. The orthogonal components are not influenced by the SLMs. After the second SLM, two plane waves exist. The one that was modulated by the SLMs can be described as

$$u_1(x, y; \vec{r}_s) = c_1(\vec{r}_s)\sqrt{I_s(\vec{r}_s)}L(\vec{r}_s/f_o) \tag{16}$$

where c_1 is a complex valued constant, dependent on the point source position, and I_s is the point source intensity. The wave that was not modulated by the SLMs can be simply described by (8). The recorded hologram for a single point source is

$$h(x, y; \vec{r}_s) = |u_1(x, y; \vec{r}_s) + u_2(x, y; \vec{r}_s)|^2 = I_s(\vec{r}_s) \left\{|c_1(\vec{r}_s)|^2 + |c_2(\vec{r}_s)|^2 + [c_1(\vec{r}_s)\, c_2^*(\vec{r}_s)\, L(-2\vec{r}_s/f_o) + \text{c.c.}]\right\} \tag{17}$$

whereas the hologram for the complete object is the summation over all point source contributions, each represented in (17). It can be shown that this hologram is of a Fourier type [6]. Specifically, each point source in the front focal plane is encoded into the hologram by a cosine fringe pattern. Considering polar coordinates, the frequency of the fringes represents the point source distance from the optical axis, and the

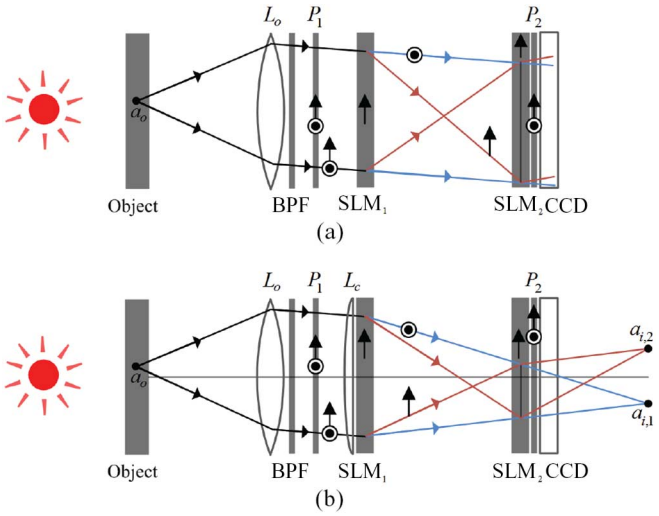

Fig. 11. Simplified schematics of FISCH. (a) First configuration of FISCH [6]. Two SLMs are shown, but a single SLM can suffice, using a mirror at the focal plane of SLM_1. (b) More recent design [50] requires two SLMs and an additional refractive lens, in order to reduce the maximal OPD. L_o, objective lens; L_c, refractive lens; BPF (optional), bandpass filter; P_1 and P_2, polarizers; SLM_1 and SLM_2, spatial light modulator; CCD, charge-coupled device.

orientation of the fringes represents its polar angle. Importantly, points located outside the front focal plane will result with added curvature to the representing fringe pattern, encoding their depth. FISCH holograms can be reconstructed by digitally calculating their inverse Fourier transform. Additional Fresnel back propagation may be used to focus into different planes. In [6], object reconstruction using a single FISCH hologram was demonstrated. Still, acquiring two holograms with a 180° relative phase shift is beneficial, to reduce the influence of the dominant zeroth-order term. A complete phase-shifting procedure, using three or more exposures may be used, but is not generally necessary.

A more recent design of FISCH that offers a reduction in maximal OPD is described in Fig. 11(b). The importance of the OPD reduction was discussed in Section III and is as relevant to FISCH as it is to FINCH. A complete description of the design is given in [50] and is not repeated herein, for the sake of brevity. Several important comments, however, should be made. The FISCH design of Fig. 11(a) can be implemented using only a single SLM and a mirror, since the two SLMs are used to display similar lenses. The FISCH design of Fig. 11(b) cannot use only a single SLM, because SLM_1 and SLM_2 are used to display lenses of different focal lengths. Further note that FINCH and FISCH maintain a very unique similarity [see Fig. 11(b) vs. Fig. 7(c), Fig. 11(a) vs. Fig. 7(b)]. Therefore, a FISCH system that is realized using two SLMs can electronically be switched into a FINCH recording mode. Using two CCDs and a beam-splitter, any FISCH system can simultaneously be used to record FINCH holograms.

A FISCH microscope based on Fig. 11(b) was implemented using a Newport M-10X objective, two Holoeye PLUTO SLMs and a PCO Edge sCMOS camera. The distance between L_o and L_c (with a focal length of 1 m) was 5 cm, and between the SLMs 55 cm. Effective distances of zero between

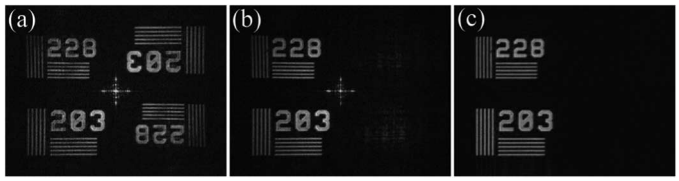

Fig. 12. Spatially incoherent holographic microscopy. (a) Target reconstruction using two FISCH holograms that differ by a 180° phase shift, showing the in-focus image and its twin. (b) Target reconstruction from a complex hologram, where the twin-image is eliminated by a complete phase-shifting procedure that uses three FISCH holograms. (c) Target reconstruction from a FINCH hologram, acquired by switching the FISCH system into a FINCH recording mode. The FISCH reconstructions in (a) and (b) were calculated using a 2-D inverse Fourier transform, whereas the FINCH reconstruction in (c) was calculated using a Fresnel back propagation.

L_c and SLM_1 and between SLM_2 and the CCD were achieved using afocal relay (4f) systems. To satisfy the perfect overlap condition, the focal lengths of the SLM displayed lenses were 61.11 and 12.38 cm for SLM_1 and SLM_2, respectively. A negative high-frequency NBS 1963A resolution chart (Thorlabs R2L2S1N1), back illuminated using a red LED (Thorlabs LED635L), served as a target. Experimental results are presented in Fig. 12, showing reconstructions from: 1) a FISCH hologram calculated from two exposures with a 180° relative phase shift; 2) a FISCH hologram from a complete phase-shifting procedure; 3) a FINCH hologram acquired by switching the system in Fig. 11(b) into FINCH recording mode, setting SLM_2 to a constant zero phase modulation.

VI. Conclusion

Three methods of holography have been reviewed herein. In a sense, FINCH, FISCH, and JORDI may be considered complementary. On one hand, they all possess a single-channel structure, unlike most other existing holography systems that usually make use of two different physical channels. This property contributes greatly to the system stability, thus rendering it applicable under various conditions. On the other hand, each of these systems can be used to record holograms of different types (Fourier, Fresnel, coherent, spatially incoherent, and etc.). Future developments, aside from the ever going efforts of improving various characteristics of the systems (e.g., lateral and axial resolution, temporal coherence requirements), may include the integration of the three methods into a single unified apparatus.

Acknowledgment

The authors would like to thank G. Brooker, B. Katz, Y. Rivenson, and N. Siegel for their part and collaboration in the various works reviewed in this paper.

References

[1] D. Gabor, "A new microscopic principle," *Nature*, vol. 161, pp. 777–778, May 1948.
[2] I. Yamaguchi and T. Zhang, "Phase-shifting digital holography," *Opt. Lett.*, vol. 22, pp. 1268–1270, Aug. 1997.
[3] T.-C. Poon, "Optical scanning holography—A review of recent progress," *J. Opt. Soc. Korea*, vol. 13, pp. 406–415, Dec. 2009.

[4] J. Rosen and G. Brooker, "Digital spatially incoherent Fresnel holography," *Opt. Lett.*, vol. 32, pp. 912–914, Apr. 2007.

[5] M. K. Kim, "Adaptive optics by incoherent digital holography," *Opt. Lett.*, vol. 37, pp. 2694–2696, Jul. 2012.

[6] R. Kelner and J. Rosen, "Spatially incoherent single channel digital Fourier holography," *Opt. Lett.*, vol. 37, pp. 3723–3725, Sep. 2012.

[7] D. N. Naik, G. Pedrini, and W. Osten, "Recording of incoherent-object hologram as complex spatial coherence function using Sagnac radial shearing interferometer and a Pockels cell," *Opt. Express*, vol. 21, pp. 3990–3995, Feb. 2013.

[8] Y. Wan, T. Man, and D. Wang, "Incoherent off-axis Fourier triangular color holography," *Opt. Express*, vol. 22, pp. 8565–8573, Apr. 2014.

[9] K. Watanabe and T. Nomura, "Recording spatially incoherent Fourier hologram using dual channel rotational shearing interferometer," *Appl. Opt.*, vol. 54, pp. A18–A22, Jan. 2015.

[10] J. Rosen and G. Brooker, "Non-scanning motionless fluorescence three-dimensional holographic microscopy," *Nat. Photon*, vol. 2, pp. 190–195, Mar. 2008.

[11] D. Weigel, H. Babovsky, A. Kiessling, and R. Kowarschik, "Widefield microscopy with infinite depth of field and enhanced lateral resolution based on an image inverting interferometer," *Opt. Commun.*, vol. 342, pp. 102–108, May 2015.

[12] Y. Hayasaki, R. Abe, and T. Yanagawa, "Three-dimensional mapping of fluorescent nanoparticles using incoherent digital holography," *Opt. Lett.*, vol. 40, pp. 3312–3315, Jul. 2015.

[13] T. Man, Y. Wan, F. Wu, and D. Wang, "Four-dimensional tracking of spatially incoherent illuminated samples using self-interference digital holography," *Opt. Commun.*, vol. 355, pp. 109–113, Nov. 2015.

[14] J. Rosen, N. Siegel, and G. Brooker, "Theoretical and experimental demonstration of resolution beyond the Rayleigh limit by FINCH fluorescence microscopic imaging," *Opt. Express*, vol. 19, pp. 26249–26268, Dec. 2011.

[15] R. Kelner and J. Rosen, "Three-dimensional imaging by self-reference digital holograms," in *Proc. 13th IEEE Int. Conf. Ind. Informat. (INDIN)*, Cambridge, U.K., to be published.

[16] Y. Rivenson, B. Katz, R. Kelner, and J. Rosen, "Single channel in-line multimodal digital holography," *Opt. Lett.*, vol. 38, pp. 4719–4722, Nov. 2013.

[17] R. Kelner, B. Katz, and J. Rosen, "Common path in-line holography using enhanced joint object reference digital interferometers," *Opt. Express*, vol. 22, pp. 4995–5009, Mar. 2014.

[18] R. Kelner and J. Rosen, "Joint object reference digital interferometer (JORDI): A single spatial light modulator based design," in *Imaging and Applied Optics*. Washington DC, USA: Optical Society of America, 2014, OSA Technical Digest (Online), paper DTu2B.6.

[19] M. Born and E. Wolf, *Principles of Optics*. Cambridge, U.K.: Pergamon Press, 1980, p. 471.

[20] J. Rosen and G. Brooker, "Fluorescence incoherent color holography," *Opt. Express*, vol. 15, pp. 2244–2250, Mar. 2007.

[21] G. Brooker, N. Siegel, J. Rosen, N. Hashimoto, M. Kurihara, and A. Tanabe "In-line FINCH super resolution digital holographic fluorescence microscopy using a high efficiency transmission liquid crystal GRIN lens," *Opt. Lett.*, vol. 38, pp. 5264–5267, Dec. 2013.

[22] B. Katz, D. Wulich, and J. Rosen, "Optimal noise suppression in Fresnel incoherent correlation holography (FINCH) configured for maximum imaging resolution," *Appl. Opt.*, vol. 49, pp. 5757–5763, Oct. 2010.

[23] G. Brooker, N. Siegel, V. Wang, and J. Rosen, "Optimal resolution in Fresnel incoherent correlation holographic fluorescence microscopy," *Opt. Express*, vol. 19, pp. 5047–5062, Mar. 2011.

[24] B. Katz and J. Rosen, "Could SAFE concept be applied for designing a new synthetic aperture telescope?," *Opt. Express*, vol. 19, pp. 4924–4936, Mar. 2011.

[25] Y. Tone, K. Nitta, O. Matoba, and Y. Awatsuji, "Analysis of reconstruction characteristics in fluorescence digital holography," in *Digital Holography and Three-Dimensional Imaging*. Washington DC, USA: Optical Society of America, 2011, OSA Technical Digest (CD), paper DTuC13.

[26] P. Bouchal, J. Kapitán, R. Chmelík, and Z. Bouchal, "Point spread function and two-point resolution in Fresnel incoherent correlation holography," *Opt. Express*, vol. 19, pp. 15603–15620, Aug. 2011.

[27] B. Katz, J. Rosen, R. Kelner, and G. Brooker, "Enhanced resolution and throughput of Fresnel incoherent correlation holography (FINCH) using dual diffractive lenses on a spatial light modulator (SLM)," *Opt. Express*, vol. 20, pp. 9109–9121, Apr. 2012.

[28] P. Bouchal and Z. Bouchal, "Selective edge enhancement in three-dimensional vortex imaging with incoherent light," *Opt. Lett.*, vol. 37, pp. 2949–2951, Jul. 2012.

[29] X. Lai, Y. Zhao, X. Lv, Z. Zhou, and S. Zeng, "Fluorescence holography with improved signal-to-noise ratio by near image plane recording," *Opt. Lett.*, vol. 37, pp. 2445–2447, Jul. 2012.

[30] N. Siegel, J. Rosen, and G. Brooker, "Reconstruction of objects above and below the objective focal plane with dimensional fidelity by FINCH fluorescence microscopy," *Opt. Express*, vol. 20, pp. 19822–19835, Aug. 2012.

[31] T. Man, Y. Wan, H. Chen, Z. Jiang, and D. Wang, "Quantitative evaluation of spatial phase light modulator characteristics in Fresnel incoherent correlation holography," in *Proc. SPIE 8556 Hologr. Diffr. Opt. Appl. V 855613*, Nov. 26, 2012, pp. 855613-1–855613-9.

[32] H. Chen, Y. Wan, T. Man, Z. Jiang, and D. Wang, "Effect of phase-shift step on hologram reconstruction in Fresnel incoherent correlation holography," in *Proc. SPIE 8556 Hologr. Diffr. Opt. Appl. V 85560L*, Nov. 26, 2012, pp. 85560L-1–85560L-9.

[33] X. Lai and S. Zeng, "Optical path difference characteristics of the fluorescence holographic system," in *Proc. SPIE 8556 Hologr. Diffr. Opt. Appl. V 855617*, Nov. 26, 2012, pp. 855617-1–855617-7.

[34] P. Bouchal and Z. Bouchal, "Wide-field common-path incoherent correlation microscopy with a perfect overlapping of interfering beams," *J. Eur. Opt. Soc. Rapid Publ.*, vol. 8, pp. 13011.1–13011.8, Jan. 2013.

[35] M. K. Kim, "Full color natural light holographic camera," *Opt. Express*, vol. 21, pp. 9636–9642, Apr. 2013.

[36] X. Lai, S. Zeng, X. Lv, J. Yuan, and L. Fu, "Violation of the Lagrange invariant in an optical imaging system," *Opt. Lett.*, vol. 38, pp. 1896–1898, Jun. 2013.

[37] K. Tsuchiya, Y. Tone, K. Nitta, O. Matoba, and Y. Awatsuji, "Influence of spatial coherence degree in fluorescence digital holography," in *Proc. Conf. Lasers Electro-Opt. Pac. Rim*, 2013, pp. 1–2, Paper WPF_30.

[38] N. Siegel, J. Rosen, and G. Brooker, "Faithful reconstruction of digital holograms captured by FINCH using a Hamming window function in the Fresnel propagation," *Opt. Lett.*, vol. 38, pp. 3922–3925, Oct. 2013.

[39] P. Bouchal and Z. Bouchal, "Concept of coherence aperture and pathways toward white light high-resolution correlation imaging," *New J. Phys.*, vol. 15, p. 123002, Dec. 2013.

[40] J. Hong and M. K. Kim, "Overview of techniques applicable to self-interference incoherent digital holography," *J. Eur. Opt. Soc. Rapid Pub.*, vol. 8, pp. 13077.1–13077.8, Dec. 2013.

[41] W. Qin *et al.*, "Fast fluorescence holographic microscopy," in *Proc. SPIE 8949 Three-Dimens. Multidimens. Microsc. Image Acquis. Process. XXI*, Mar. 12, 2014, p. 89491W.

[42] Y.-H. Wan, T.-L. Man, H. Chen, Z.-Q. Jiang, and D.-Y. Wang, "Effect of wavefront properties on numerical aperture of Fresnel hologram in incoherent holographic microscopy," *Chin. Phys. Lett.*, vol. 31, no. 4. p. 044203–1, Apr. 2014.

[43] W. Qin *et al.*, "Two-step phase-shifting fluorescence incoherent holographic microscopy," *J. Biomed. Opt.*, vol. 19, p. 060503, Jun. 2014.

[44] R. Kelner, B. Katz, and J. Rosen, "Optical sectioning using a digital Fresnel incoherent-holography-based confocal imaging system," *Optica*, vol. 1, pp. 70–74, Aug. 2014.

[45] Y. Kashter and J. Rosen, "Enhanced-resolution using modified configuration of Fresnel incoherent holographic recorder with synthetic aperture," *Opt. Express*, vol. 22, pp. 20551–20565, Aug. 2014.

[46] N. Siegel and G. Brooker, "Improved axial resolution of FINCH fluorescence microscopy when combined with spinning disk confocal microscopy," *Opt. Express*, vol. 22, pp. 22298–22307, Sep. 2014.

[47] J. Rosen and R. Kelner, "Modified Lagrange invariants and their role in determining transverse and axial imaging resolutions of self-interference incoherent holographic systems," *Opt. Express*, vol. 22, pp. 29048–29066, Nov. 2014.

[48] A. W. Lohmann, "Wavefront reconstruction for incoherent objects," *J. Opt. Soc. Amer.*, vol. 55, pp. 1555–1556, Nov. 1965.

[49] G. Cochran, "New method of making Fresnel transforms with incoherent light," *J. Opt. Soc. Amer.*, vol. 56, pp. 1513–1517, Nov. 1966.

[50] R. Kelner, J. Rosen, and G. Brooker, "Enhanced resolution in Fourier incoherent single channel holography (FISCH) with reduced optical path difference," *Opt. Express*, vol. 21, pp. 20131–20144, Aug. 2013.

[51] E. Wolf, *Introduction to the Theory of Coherence and Polarization of Light*. Cambridge, U.K.: Cambridge Univ. Press, 2007.

[52] M. Minsky, "Memoir on inventing the confocal scanning microscope," *Scanning*, vol. 10, pp. 128–138, 1988.

[53] S. Lai, R. A. McLeod, P. Jacquemin, S. Atalick, and R. Herring, "An algorithm for 3-D refractive index measurement in holographic confocal microscopy," *Ultramicroscopy*, vol. 107, pp. 196–201, Feb. 2007.

[54] A. S. Goy and D. Psaltis, "Digital confocal microscope," *Opt. Express*, vol. 20, pp. 22720–22727, Sep. 2012.

[55] C. Liu, S. Marchesini, and M. K. Kim, "Quantitative phase-contrast confocal microscope," *Opt. Express*, vol. 22, pp. 17830–17839, Jul. 2014.
[56] P.-C. Sun and E. N. Leith, "Broad-source image plane holography as a confocal imaging process," *Appl. Opt.*, vol. 33, pp. 597–602, Feb. 1994.
[57] R. Chmelík and Z. Harna, "Parallel-mode confocal microscope," *Opt. Eng.*, vol. 38, pp. 1635–1639, Oct. 1999.

Roy Kelner received the B.Sc. (*magna cum laude*), M.Sc. (*magna cum laude*), and Ph.D. degrees in electrical and computer engineering from Ben-Gurion University of the Negev, Beer-Sheva, Israel, in 2008, 2010, and 2015, respectively.

Currently, he is a Postdoctoral Fellow with the Department of Electrical and Computer Engineering, Ben-Gurion University of the Negev.

Joseph Rosen received the B.Sc., M.Sc., and D.Sc. degrees in electrical engineering from the Technion-Israel Institute of Technology, Haifa, Israel, in 1984, 1987, and 1992, respectively.

He is a Benjamin H. Swig Professor of Optoelectronics with the Department of Electrical and Computer Engineering, Ben-Gurion University of the Negev, Beer-Sheva, Israel. He has co-authored approximately 200 scientific journal papers, book chapters, and conference publications. His research interests include digital holography, optical microscopy, diffractive optics, statistical optics, biomedical optics, optical computing, and image processing.

Dr. Rosen is a Fellow of the Optical Society of America and the International Society for Optical Engineering.